HOKKAIDO UNIVERSITY

Title	DYNAMIC SOIL-STRUCTURE INTERACTION ANALYSIS IN THE FINITE ELEMENT TIME DOMAIN WITH CONVOLUTIONAL PERFECTLY MATCHED LAYER AS THE BOUNDARY CONDITIONS
Author(s)	XU, BO-QING; TSANG, HING-HO; LO, S. H.
Description	The Thirteenth East Asia-Pacific Conference on Structural Engineering and Construction (EASEC-13), September 11-13, 2013, Sapporo, Japan.
Relation	Proceedings of the Thirteenth East Asia-Pacific Conference on Structural Engineering and Construction (EASEC-13), September 11-13, 2013, Sapporo, Japan, I-3-4.
Citation	Proceedings of the Thirteenth East Asia-Pacific Conference on Structural Engineering and Construction (EASEC-13), I-3-4
Issue Date	2013-09-13
Doc URL	https://hdl.handle.net/2115/54487
Type	conference paper
File Information	easec13-I-3-4.pdf

Hokkaido University Collection of Scholarly and Academic Papers : HUSCAP

DYNAMIC SOIL-STRUCTURE INTERACTION ANALYSIS IN THE FINITE ELEMENT TIME DOMAIN WITH CONVOLUTIONAL PERFECTLY MATCHED LAYER AS THE BOUNDARY CONDITIONS

Bo-Qing Xu[*†], Hing-Ho Tsang and S. H. Lo

Department of Structural Engineering, The University of Hong Kong, Hong Kong

ABSTRACT

Convolutional perfectly matched layer (CPML) models in the finite element time domain (FETD) can save computational costs when the original problem domain is relatively large or where three-dimensional (3-d) modeling is needed. The use of CPML for solving soil-structure interaction (SSI) problems in truncated domains using finite element method has been explored in this paper. It provides a method of applying CPML models to dynamic SSI analysis in FETD with displacement as the only unknown. Relevant benchmark examples with small bounded domains have been included to demonstrate the stability and efficiency of the proposed model and formulation. An interesting application of this technique can also be found about the classical SSI problem of evaluating the responses of the building with rigid footing on a half-space under earthquake motions.

Keywords: Perfectly matched layer, absorbing boundary, soil-structure interaction, finite element time domain, bounded domains.

1. INTRODUCTION

The concept of a perfectly matched layer (PML) was first introduced to electromagnetic waves (Berenger 1994). The PML was then defined in the viewpoint of a complex stretched coordinate (Chew and Weedon 1994). After that, the application of PML as an efficient absorbing boundary condition has been widely explored (Chew and Liu 1996). However, most of the studies and applications are connected to finite difference time domain (FDTD). Since existing software for finite element modeling of solid mechanics and elasticity problems usually solves for displacement only in FETD, there is a need for developing a PML formulation of FETD with only displacement as unknown for the elastic second order wave equation (SOWE), which is also known as the governing equation of SSI problems. To the authors' knowledge, some attempts to solve the above problem have been reported. Basu almost established an FE discretized SOWE for the displacement (Basu and Chopra 2004), though the formulation involves tricky coordinate transformations of the

[*] Corresponding author: Email: xuboqing@hku.hk

[†] Presenter: Telephone: 852-69930656

displacement gradients to compute the strains. A CPML model for the SOWE using auxiliary memory variables was demonstrated (Li and Matar 2010) to avoid the convolution operators. Another recent work in (Matzen 2011) suggests a non-split variational formulation of the CPML for elastic SOWE with displacement as the single unknown. It shows the possibility of FE implementation of an efficient CPML to existing displacement based FE codes to solve open-region dynamic SSI problems. This paper presents a 3-d CPML model for dynamic SSI analysis in the FETD with displacement as the only unknown. The stability and efficiency of the proposed formulation are demonstrated by relevant examples including an interesting application to the classical SSI problem of a building with rigid footing on layers on a half-space.

2. CPML EQUATIONS

The key concept of the PML is a complex frequency coordinate stretching, which maps the spartial variables onto a complex space by a complex coordinate stretching function. In a 3-d space, this function can be defined as

$$\hat{x}_i = \int_0^{x_i} s_i(\tilde{x}_i, \omega)\, \mathrm{d}\tilde{x}_i, \quad i = 1,2,3 \tag{1}$$

where ω is the angular frequency and s_i are the stretched coordinate metrics proposed (Kuzuoglu and Mittra 1996)

$$s_i(x_i, \omega) = \kappa_i(x_i) + \frac{\beta_i(x_i)}{\alpha_i(x_i) + j\omega}, \quad i = 1,2,3 \tag{2}$$

Where j is the imaginary unit and κ_i, α_i and β_i are the coordinate-wise non-negative real function that controls the attenuation of the propagating waves. At the interface of the computational domain and the PML domain, $\kappa_i = 1$ and $\beta_i = 0$. For the standard PML, $\kappa_i = 1$ and $\alpha_i = 0$ in Equation (2). For the CPML, the real function $\kappa_i \geqslant 1$ and the imaginary function $\beta_i / (\alpha_i + j\omega)$ serve to enhance attenuation of evanescent and the near-grazing waves. It is known that wave propagation in a linear elastic medium is governed by the motion equation, the strain-displacement equations and the constitutive equations. By introducing the complex stretched function of Equation (1) into the frequency domain counterparts of the governing equations and then applying the inverse Fourier transform, one can get the time domain equation of motion and the displacement based constitutive equations for the CPML domain as follows

$$\begin{aligned} \nabla \cdot \boldsymbol{\sigma} + \rho \mathbf{p} &= \Psi_0(t)\ddot{\mathbf{u}} \\ \boldsymbol{\sigma} &= \mathbf{C}\partial\mathbf{u} \\ \mathbf{C} &= \sum_{i=1}^{6} \boldsymbol{\Psi}_i(t)\mathbf{C}_i \end{aligned} \tag{3}$$

where $\boldsymbol{\sigma}$ and $\mathbf{C}$ are the stress and stiffness tensors, respectively, ρ represents the mass density, $\mathbf{u}$ and $\ddot{\mathbf{u}}$ are the displacement and acceleration vectors, respectively, and $\mathbf{p}$ is the body force vector. The six matrices $\mathbf{C}_i$ are given as follows

$$\mathbf{C}_1=\begin{bmatrix}0&0&0&0&0&0&0&0&0\\0&0&\lambda&0&0&0&0&0&0\\0&\lambda&0&0&0&0&0&0&0\\0&0&0&0&0&0&0&0&0\\0&0&0&0&0&0&0&0&0\\0&0&0&0&0&\frac{\mu}{2}&0&0&0\\0&0&0&0&0&0&0&0&0\\0&0&0&0&0&0&0&0&0\\0&0&0&0&0&0&0&0&-\frac{\mu}{2}\end{bmatrix},\mathbf{C}_2=\begin{bmatrix}0&0&\lambda&0&0&0&0&0&0\\0&0&0&0&0&0&0&0&0\\\lambda&0&0&0&0&0&0&0&0\\0&0&0&0&0&0&0&0&0\\0&0&0&0&\frac{\mu}{2}&0&0&0&0\\0&0&0&0&0&0&0&0&0\\0&0&0&0&0&0&0&0&0\\0&0&0&0&0&0&0&-\frac{\mu}{2}&0\\0&0&0&0&0&0&0&0&0\end{bmatrix}$$

$$\mathbf{C}_3=\begin{bmatrix}0&\lambda&0&0&0&0&0&0&0\\\lambda&0&0&0&0&0&0&0&0\\0&0&0&0&0&0&0&0&0\\0&0&0&\frac{\mu}{2}&0&0&0&0&0\\0&0&0&0&0&0&0&0&0\\0&0&0&0&0&0&0&0&0\\0&0&0&0&0&0&-\frac{\mu}{2}&0&0\\0&0&0&0&0&0&0&0&0\\0&0&0&0&0&0&0&0&0\end{bmatrix},\mathbf{C}_4=\begin{bmatrix}0&0&0&0&0&0&0&0&0\\0&0&0&0&0&0&0&0&0\\0&0&2\mu+\lambda&0&0&0&0&0&0\\0&0&0&0&0&0&0&0&0\\0&0&0&0&\frac{\mu}{4}&0&0&-\frac{\mu}{4}&0\\0&0&0&0&0&\frac{\mu}{4}&0&0&-\frac{\mu}{4}\\0&0&0&0&0&0&0&0&0\\0&0&0&0&-\frac{\mu}{4}&0&0&\frac{\mu}{4}&0\\0&0&0&0&0&-\frac{\mu}{4}&0&0&\frac{\mu}{4}\end{bmatrix}$$

$$\mathbf{C}_5=\begin{bmatrix}0&0&0&0&0&0&0&0&0\\0&2\mu+\lambda&0&0&0&0&0&0&0\\0&0&0&0&0&0&0&0&0\\0&0&0&\frac{\mu}{4}&0&0&-\frac{\mu}{4}&0&0\\0&0&0&0&0&0&0&0&0\\0&0&0&0&0&\frac{\mu}{4}&0&0&\frac{\mu}{4}\\0&0&0&-\frac{\mu}{4}&0&0&\frac{\mu}{4}&0&0\\0&0&0&0&0&0&0&0&0\\0&0&0&0&0&\frac{\mu}{4}&0&0&\frac{\mu}{4}\end{bmatrix},\mathbf{C}_6=\begin{bmatrix}2\mu+\lambda&0&0&0&0&0&0&0&0\\0&0&0&0&0&0&0&0&0\\0&0&0&0&0&0&0&0&0\\0&0&0&\frac{\mu}{4}&0&0&\frac{\mu}{4}&0&0\\0&0&0&0&\frac{\mu}{4}&0&0&\frac{\mu}{4}&0\\0&0&0&0&0&0&0&0&0\\0&0&0&\frac{\mu}{4}&0&0&\frac{\mu}{4}&0&0\\0&0&0&0&\frac{\mu}{4}&0&0&\frac{\mu}{4}&0\\0&0&0&0&0&0&0&0&0\end{bmatrix}$$

where λ and μ are the Lamé parameters. The seven operators Ψ_i are generated by the process of the inverse Fourier transform, which are respectively given by

$$\Psi_0(t)=P_0\frac{\partial^2}{\partial t^2}+P_1\frac{\partial}{\partial t}+P_2+\alpha_1^2\beta_1P_{3,12}P_{3,13}e^{-\alpha_1 t}H(t)*+\alpha_2^2\beta_2P_{3,21}P_{3,23}e^{-\alpha_2 t}H(t)*+\alpha_3^2\beta_3P_{3,31}P_{3,32}e^{-\alpha_3 t}H(t)* \quad (4)$$

$$\Psi_n(t)=\kappa_n+\beta_ne^{-\alpha_n t}H(t)* \quad (n=1,2,3) \quad (5)$$

$$\Psi_4(t)=\kappa_1\kappa_2\kappa_3^{-1}+\beta_1P_{3,12}P_{3,13}^{-1}e^{-\alpha_1 t}H(t)*+\beta_2P_{3,21}P_{3,23}^{-1}e^{-\alpha_2 t}H(t)*-\beta_3\kappa_3^{-2}P_{4,31}P_{4,32}e^{-(\kappa_3\alpha_3+\beta_3)t/\kappa_3}H(t)* \quad (6)$$

$$\Psi_5(t)=\kappa_1\kappa_2^{-1}\kappa_3+\beta_1P_{3,13}P_{3,12}^{-1}e^{-\alpha_1 t}H(t)*+\beta_3P_{3,31}P_{3,32}^{-1}e^{-\alpha_3 t}H(t)*-\beta_2\kappa_2^{-2}P_{4,21}P_{4,23}e^{-(\kappa_2\alpha_2+\beta_2)t/\kappa_2}H(t)* \quad (7)$$

$$\Psi_6(t)=\kappa_1^{-1}\kappa_2\kappa_3+\beta_2P_{3,23}P_{3,21}^{-1}e^{-\alpha_2 t}H(t)*+\beta_3P_{3,12}P_{3,13}^{-1}e^{-\alpha_3 t}H(t)*-\beta_1\kappa_1^{-2}P_{4,12}P_{4,13}e^{-(\kappa_1\alpha_1+\beta_1)t/\kappa_1}H(t)* \tag{8}$$

where $H(t)$ is the Heaviside step function, * denotes the temporal convolution and P_0, P_1, P_2, $P_{3,i}$ and $P_{4,i}$ are the spatially varying functions which are introduced as follows

$$\begin{aligned}
P_0 &= \kappa_1\kappa_2\kappa_3 \\
P_1 &= \kappa_2\kappa_3\beta_1+\kappa_1\kappa_3\beta_2+\kappa_1\kappa_2\beta_3 \\
P_2 &= \kappa_1\beta_2\beta_3+\kappa_2\beta_1\beta_3+\kappa_3\beta_1\beta_2-\alpha_1\kappa_2\kappa_3\beta_1-\alpha_2\kappa_1\kappa_3\beta_2-\alpha_3\kappa_1\kappa_2\beta_3 \\
P_{3,ij} &= [\kappa_j(\alpha_i-\alpha_j)-\beta_j]/(\alpha_i-\alpha_j) \quad (i,j=1,2,3 \text{ and } i\neq j) \\
P_{4,ij} &= [\kappa_i\kappa_j(\alpha_i-\alpha_j)+\kappa_j\beta_i-\kappa_i\beta_j]/[\kappa_i(\alpha_i-\alpha_j)+\beta_i] \quad (i,j=1,2,3 \text{ and } i\neq j)
\end{aligned} \tag{9}$$

The parameters κ_i, α_i and β_i of the CPML can be chosen as suggests (Collino and Monk 1998). By separating the convolution terms in Equation (3), adding the external load and expanding the displacement field using FEM, one can obtain the ordinary differential equation

$$\mathbf{M}\ddot{\mathbf{d}}+\mathbf{D}\dot{\mathbf{d}}+\mathbf{K}\mathbf{d}=\mathbf{f}+\mathbf{h}+\mathbf{g} \tag{10}$$

where $\mathbf{d}$, $\dot{\mathbf{d}}$ and $\ddot{\mathbf{d}}$ are the unknown displacement, velocity and acceleration vectors, respectively. **M**, **D** and **K** are the global mass, damping and stiffness matrices which are assembled from their corresponding element matrices $\mathbf{M}^{\mathrm{e}}$, $\mathbf{D}^{\mathrm{e}}$ and $\mathbf{K}^{\mathrm{e}}$:

$$\begin{aligned}
\mathbf{M}^{\mathrm{e}} &= \int_{\Omega^{\mathrm{e}}}\rho P_0\mathbf{N}^{\mathrm{T}}\mathbf{N}\,\mathrm{d}\Omega \\
\mathbf{D}^{\mathrm{e}} &= \int_{\Omega^{\mathrm{e}}}\rho P_1\mathbf{N}^{\mathrm{T}}\mathbf{N}\,\mathrm{d}\Omega \\
\mathbf{K}^{\mathrm{e}} &= \int_{\Omega^{\mathrm{e}}}\mathbf{B}^{\mathrm{T}}\left(\kappa_1\mathbf{C}_1+\kappa_2\mathbf{C}_2+\kappa_3\mathbf{C}_3+\frac{\kappa_1\kappa_2}{\kappa_3}\mathbf{C}_4+\frac{\kappa_1\kappa_3}{\kappa_2}\mathbf{C}_5+\frac{\kappa_2\kappa_3}{\kappa_1}\mathbf{C}_6\right)\mathbf{B}\,\mathrm{d}\Omega+\int_{\Omega^{\mathrm{e}}}\rho P_2\mathbf{N}^{\mathrm{T}}\mathbf{N}\,\mathrm{d}\Omega
\end{aligned} \tag{11}$$

f and **h** are the global external force and body force vectors, respectively, and **g** is the global convolution vector which contains the temporal convolutions and can be recursively updated (Abenius et al. 2005). Here, $\mathbf{B}=\partial\mathbf{N}$ and the sub-matrix of **B**, $\mathbf{B}_j$, now reads as

$$\mathbf{B}_j=\begin{bmatrix}
N_{j,1} & 0 & 0 & N_{j,2} & N_{j,3} & 0 & N_{j,2} & N_{j,3} & 0 \\
0 & N_{j,2} & 0 & N_{j,1} & 0 & N_{j,3} & -N_{j,1} & 0 & N_{j,3} \\
0 & 0 & N_{j,3} & 0 & N_{j,1} & N_{j,2} & 0 & -N_{j,1} & -N_{j,2}
\end{bmatrix}^{\mathrm{T}} \tag{12}$$

After adopting the Newmark average acceleration method (Hughes 1987) for numerical time integration, the following equation can be derived for solving the displacement at each time step Δt:

$$\begin{aligned}
\left(\frac{1}{4}\mathbf{K}+\frac{1}{\Delta t^2}\mathbf{M}+\frac{1}{2\Delta t}\mathbf{D}\right)\mathbf{d}_{t+\Delta t} &= -\left[\frac{1}{2}\mathbf{K}-\frac{2}{\Delta t^2}\mathbf{M}\right]\mathbf{d}_t-\left(\frac{1}{4}\mathbf{K}+\frac{1}{\Delta t^2}\mathbf{M}-\frac{1}{2\Delta t}\mathbf{D}\right)\mathbf{d}_{t-\Delta t} \\
&+\frac{1}{4}\mathbf{f}_{t+\Delta t}+\frac{1}{2}\mathbf{f}_t+\frac{1}{4}\mathbf{f}_{t-\Delta t}+\frac{1}{4}\mathbf{h}_{t+\Delta t}+\frac{1}{2}\mathbf{h}_t+\frac{1}{4}\mathbf{h}_{t-\Delta t}+\frac{1}{4}\mathbf{g}_{t+\Delta t}+\frac{1}{2}\mathbf{g}_t+\frac{1}{4}\mathbf{g}_{t-\Delta t}
\end{aligned} \tag{13}$$

which is unconditionally stable and in the second order of accuracy.

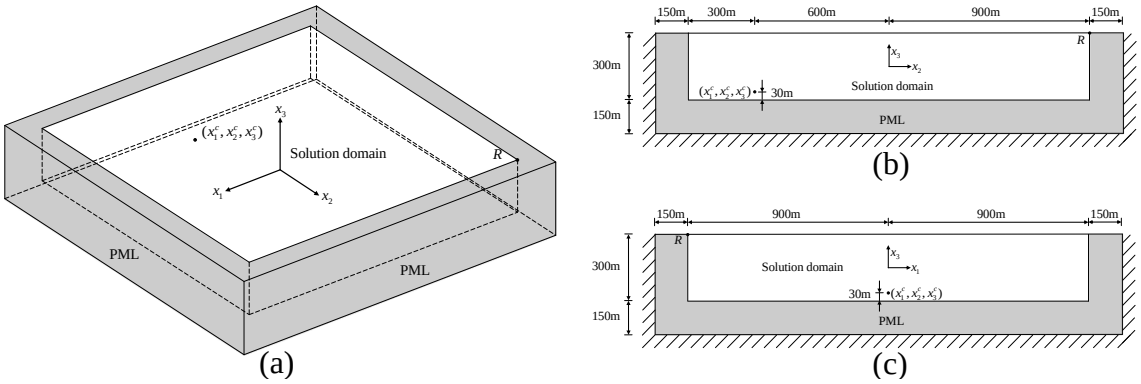

Figure 1: C-PML model for a three dimensional domain subjected to a point source.

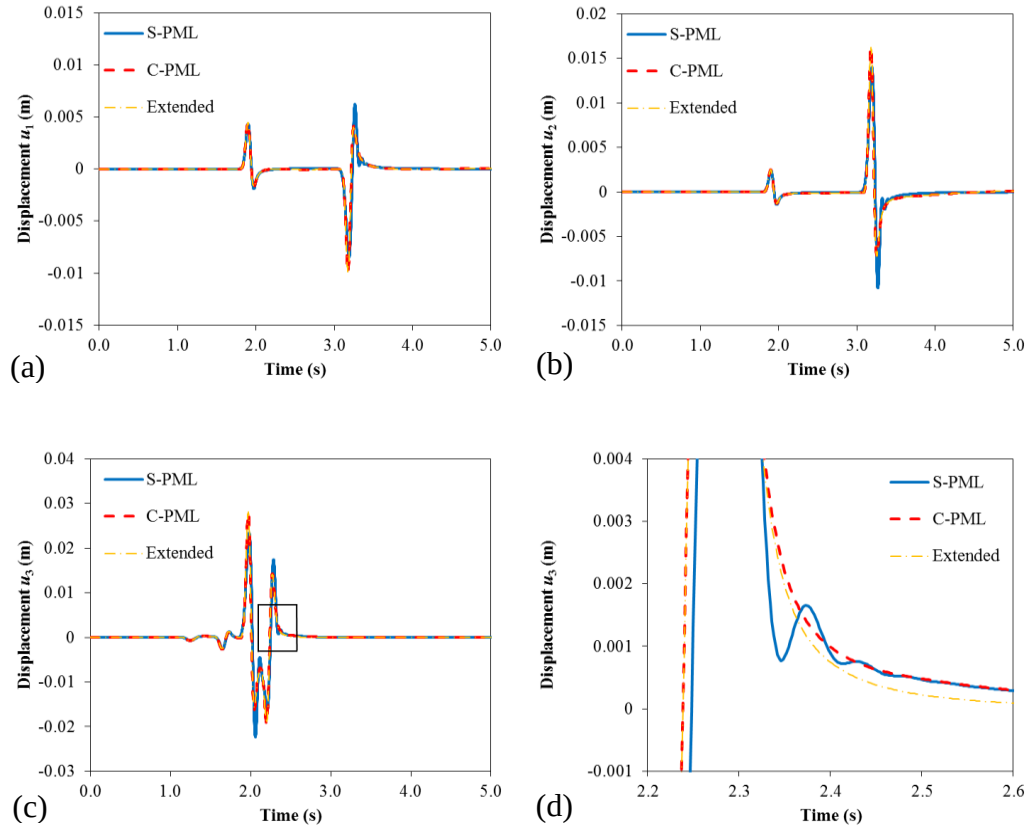

Figure 2: Comparison of the results at the receiving position *R*.

3. EXAMPLES

3.1. Single point source

In this example, to demonstrate the excellent absorbing properties of the 3-d CPML suggested, a computational domain of 1800 m × 1800 m × 300 m with a top free surface is used, which is truncated by a 150 m thick CPML as illustrated in Figure 1. For the sake of simplicity, it is assumed

that the materials are homogeneous, with the density $\rho = 16500\,\text{kg/m}^3$, the primary wave velocity v_p = 1000 m/s, and the shear wave velocity v_s = 577 m/s. The source is located at the position of (0 m, −600 m, −120 m) driven by an explosive Ricker wavelet.

Figure 2 shows the displacement responses, u_1, u_2 and u_3, at the receiver R located at the position of (−900 m, 900 m, 150 m). In all plots, the responses based on the standard PML (SPML) model implementation (i.e. for $\alpha_i = 0$ and $\kappa_i = 1$) and those based on an extended model with 4 times of the domain size are also included. If the domain is large enough that there is no reflected wave motion in the time period interested, the extended domain solution in that period can be regarded as the exact solution. Clearly, both the SPML and the CPML strategies perform almost equally and quite close to the extended domain solution in this example. Figure 2(d) is the local enlargement of the rectangular in Figure 2(c), which shows that the CPML is more capable of attenuating the evanescent field than the SPML.

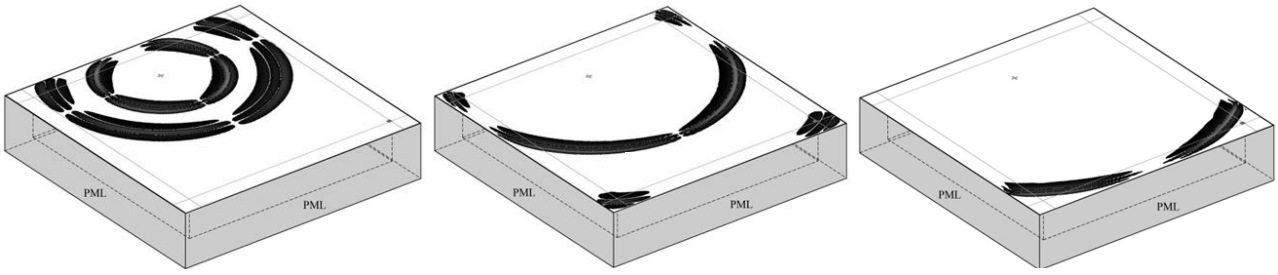

(a) 1.0 s (b) 2.0 s (c) 3.0 s

Figure 3: Snapshots of Example 1 at the top free surface

The wave motion snapshots at the top free surface are shown in Figure 3. When the wave-front reaches the CPML boundary after 1.0 s, there is no obviously reflected wave motion observed. The absorption capacity of the CPML boundary is verified.

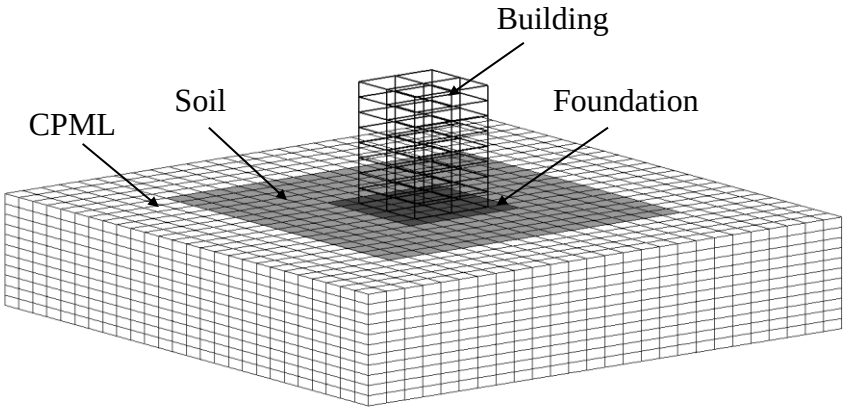

Figure 4: Finite element model of the soil-foundation-structure system with CPML

3.2. Building responses under earthquake motion

Typical soil-structure interaction model is used in this example as shows in Figure 4. The building structure on a 2 m thick concrete foundation has a height of 24 m. It is 8m in both of the other two dimensions. The superstructure is modeled by an assembly of three-dimensional frame elements. For the foundation and subsoil materials, eight-node solid elements are used in the modeling. In order to simulate the non-reflective effects of the infinite soil transmitting half-space, the model of CPML has been used as the boundary of the computational domain.

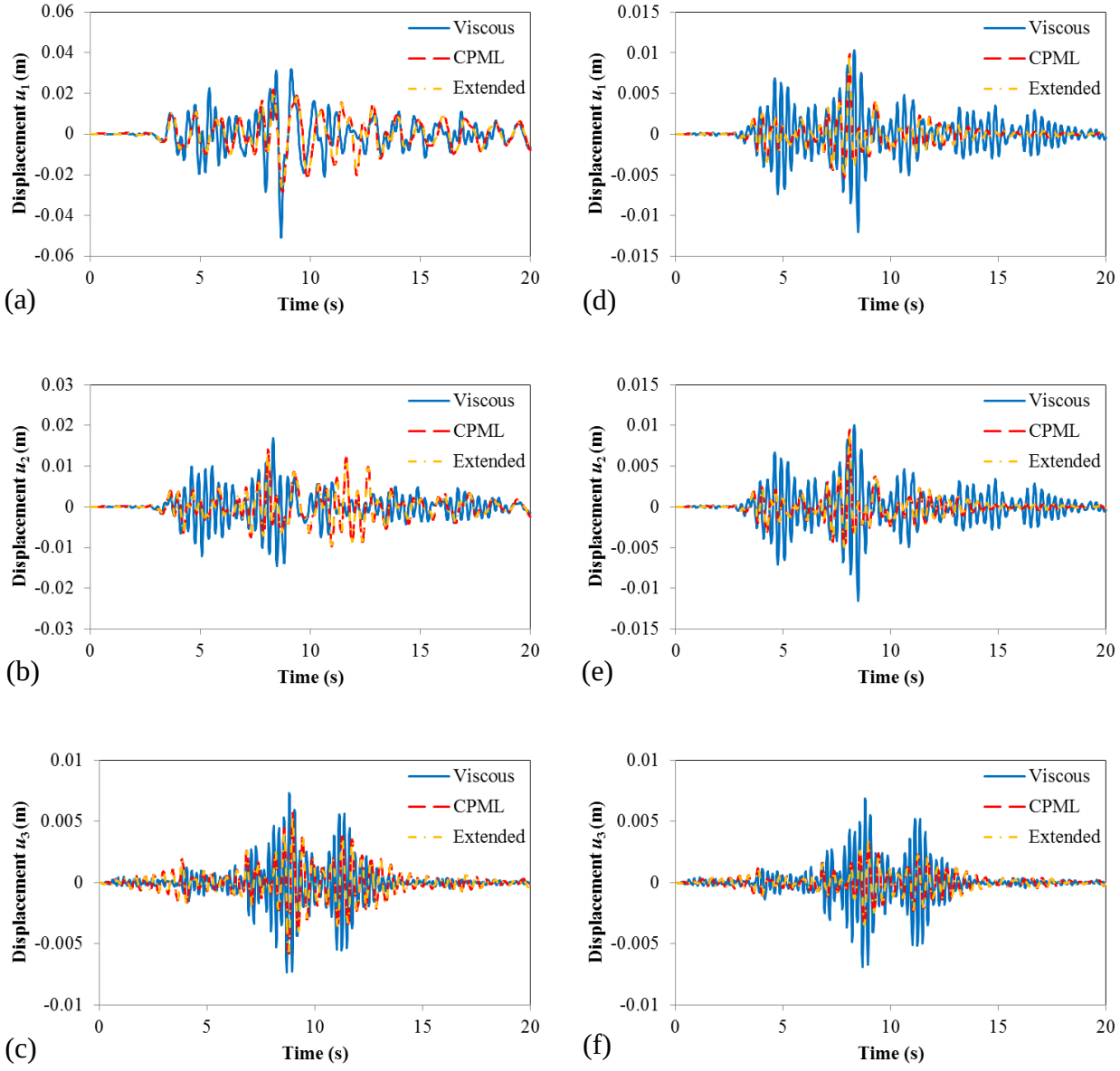

Figure 5: Responses of the roof of the building (left) and the center of the footing (right)

The numerical analysis is conducted by reducing the soil system to a computational domain of 32m×32m×12m surrounded by 10m thick CPML. An earthquake ground motion of time histories is applied at the depth of 10m from the ground surface. The displacement responses of the center of

the footing and the roof of the building are recorded. The result of the simulation with CPML model is plotted in Figure 5, compared to that from an extended model of 320m×320m×120m and that from a model with viscous boundary. It can be seen from Figure 5 that the result from the CPML model is quite close to that from the extended model, while the viscous boundary does not absorb as much wave motion as CPML does.

4. CONCLUSIONS

The primary purpose of this paper is to show the possibility to implement the CPML model to the analyses of SSI problems, when existing displacement based finite element codes need to be used to handle open-region or large domain problems. It is demonstrated by numerical examples that the accuracy of the developed model and formulation is quite high.

REFERENCES

Abenius E, Edelvik F, and Johansson C (2005). Waveguide truncation using UPML in the finite element time domain method. Technical Report 026. doi: 10.1.1.142.1839

Basu U and Chopra AK (2004). Perfectly matched layers for transient elastodynamics of unbounded domains. International Journal for Numerical Methods in Engineering. 61(1), pp. 156-157.

Berenger JP (1994). A perfectly matched layer for the absorption of electromagnetic waves. Journal of Computational Physics, 114(2). pp. 185-200.

Chew WC and Liu QH. (1996). Perfectly matched layers for elastodynamics: A new absorbing boundary condition. Journal of Computational Acoustics, 4(4), pp. 341-359.

Chew WC and Weedon WH (1994). A 3d perfectly matched medium from modified Maxwells equations with stretched coordinates. Microwave and Optical Technology Letters. 7(13), pp. 599-604.

Collino F and Monk PB (1998). Optimizing the perfectly matched layer. Computer Methods in Applied Mechanics and Engineering. 164(1-2), pp. 157-171.

Hughes TJR (1987). The Finite Element Method: Linear Static and Dynamic Finite Element Analysis. Prentice Hall Englewood Cliffs, NJ.

Kuzuoglu M and Mittra R (1996). Frequency dependence of the constitutive parameters of causal perfectly matched anisotropic absorbers. IEEE Microwave and Guided Wave Letters. 6(12), pp. 447-449.

Li YF and Matar OB (2010). Convolutional perfectly matched layer for elastic second order wave equation. Journal of the Acoustical Society of America. 127(3), pp. 1318-1327.

Matzen R (2011). An efficient finite element time-domain formulation for the elastic second-order wave equation: a non-split complex frequency shifted convolutional PML. International Journal for Numerical Methods in Engineering. 88(10), pp. 951-973.